arXiv:cond-mat/0209438v1 [cond-mat.mes-hall] 18 Sep 2002

A comparative study of some models of incoherence at the mesoscopic scale.

Colin Benjamin* and A. M. Jayannavar†

Institute of Physics, Sachivalaya Marg,

Bhubaneswar 751 005, Orissa, India

(Dated: March 22, 2022)

Abstract

The pre-existing literature on phenomena at the mesoscopic scale is concerned among other things with phase coherent transport. Phase coherent transport dominates at very low temperatures. With increase in temperature, as the system size becomes comparable to the inelastic mean free path phase incoherence sets in. This incoherence further leads to dephasing, and as a consequence purely quantum effects in electron transport give way to classical macroscopic behavior. In this work we consider two distinct phenomenological models of incoherent transport, the Coherent Absorption and Wave Attenuation models. We reveal some physical problems in the Coherent Absorption model as opposed to the Wave Attenuation model. We also compare our proposed model with experiments in case of the much studied peak to valley ratios in resonant tunneling diodes, magneto-conductance oscillations and Fano resonances in case of Aharonov-Bohm rings.

PACS numbers: 72.10.-d, 73.23.-b, 05.60.Gg, 85.35.Ds

Keywords: Inelastic Scattering, Resonant tunneling Diodes, Aharonov-Bohm rings, Fano resonances

I. INTRODUCTION

Absorption of particles has been long studied in quantum mechanics[1]. In many quantum mechanical scattering experiments there is absorption of the incident beam; the target particle may get excited, or change it's state or another particle may emerge (if it isn't a fundamental particle). Here Absorption implies inelastic scattering which can be simulated phenomenologically in the Schroedinger equation by means of a complex potential, sometimes called optical potential in nuclear physics literature[2,3,4]. The Hamiltonian becomes non-hermitian and there is no particle number conservation. Hence forth known as Coherent Absorption. The method of Coherent Absorption has also been utilized to study the localization of waves in a random media in presence of absorbing/amplifying medium[5]. It should be noted that absorption should not be confused with disappearance of particles, which is unacceptable. However absorption should be treated as particles that have entered into different inelastic channels, or loss of particles from the coherent channel. This is not the only way in which absorption induced inelastic scattering can be simulated. The other method is Wave Attenuation, which has been earlier utilized to study problems relating to 1D localization[6] and dephasing of Aharonov-Bohm oscillations[7]. Both of these models have been used to calculate quantum mechanically the conditional sojourn times taken by a particle to traverse a region of interest[8,9]. In the not so distant past, some experimental studies[10] were performed on neutron interferometry to bring out the effect of different types of absorption. In section II, we give brief definitions and also bring out the differences in the above phenomenological models of incoherence.

The reason we are interested in absorption in mesoscopic systems is due to the fact that incoherent transport plays an important role in these systems. Of course, Landauer has demonstrated[11] since long that the conductance of these systems, with elastic scattering alone, can be obtained from the transmission probability of the sample, that is it's overall scattering matrix. In a realistic model, however, phase breaking processes have to be taken into account which destroy the quantum coherence and lead to dissipation[12]. Such effects can be phenomenologically included into the Landauer picture by the models of absorption considered above.

II. MODELS OF INCOHERENCE

Incoherence in particle transport can be modeled in several ways. Among the first was by Büttiker[13,14] who considered an electron reservoir coupled by a lead to a mesoscopic system as a phase breaker or inelastic scatterer (voltage probe). This approach has been widely used to investigate the effect of incoherence or dephasing on the conductance. This method which uses voltage probes as dephasor's is interesting because of it's conceptual clarity and it's close relation to experiments. It provides a useful trick to simulate lack of full coherence in transport properties. This method of addressing the problem of dephasing has the advantage that inelastic phase randomizing processes can be incorporated by solving an elastic time independent scattering problem. Beyond Büttiker's model, Coherent Absorption[3,15] and Wave Attenuation models[6,7] have also been used to simulate dephasing. However, in the aforesaid models energy relaxation and thermal effects[16] are ignored. Thermal effects can be incorporated by taking into account thermal distribution (Fermi-Dirac function) of electrons. In mesoscopic systems, transmission functions are more often than not constant over the energy range wherein transport occurs (at low temperatures) and one can ignore energy relaxation or "vertical flow"[17] of electron carrier's in these systems. Brouwer and Beenakker have corrected some of the problems associated with voltage probe and Coherent Absorption models, (see Refs.[7,18] for details), and given a general formalism for calculating the conductance(G) in the presence of inelastic scattering. Furthermore, methods based on Coherent Absorption and Wave Attenuation can make use of this above formalism.

In this work we compare the method of Coherent Absorption and Wave Attenuation models. For this we study some topics in mesoscopic physics wherein to model inelastic scattering recourse to such models of absorption is often implied. Two representative topics wherein we apply these absorptive models are Resonant tunneling diodes(RTD) and Aharonov-Bohm(AB) rings. In RTD's, the discrepancy between experimental and theoretical peak to valley ratios has often been attributed to incoherent or sequential transport[19,20]. We model incoherent transport through both of these models of absorption and point out certain problems with the Coherent Absorption model as compared to the Wave Attenuation model. In AB rings also the same anomalies with regard to the Coherent Absorption model are put forth through some representative plots of conductance. Some aspects of dephasing on AB oscillations are discussed. Further we utilize the method of Wave Attenuation to

model incoherent transport and explain the transition of Fano to Lorentzian line shapes obtained in the Conductance of an Aharonov-Bohm ring with a symmetrically placed quantum dot on it's upper arm.

III. RESONANT TUNNELING DIODES

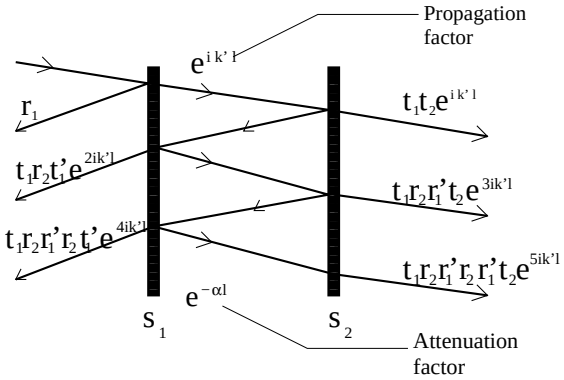


FIG. 1: Summing the different paths, S_1 and S_2 denote the two scatterer's. l is the distance between them. $e^{ik'l}$ and $e^{-\alpha l}$ denote the propagation and attenuation factors in the locality of interest.

Technological progress in semiconductor fabrication has led to the possibility of devices which are based on quantum effects. A simple such device is the double barrier diode[21,22,23], analogous to the model of a Fabry-Perot interferometer as in FIG. 1. It consists of two potential barriers separated by a thin quantum well. The transmission of electrons across this diode shows sharp resonances when energy of incident electrons are close to that of a quasi bound state. FIG. 2 shows a double barrier diode wherein a quantum well (region III) is sandwiched between two equal barrier's II and IV. Region's I and V denote electrodes. Here incident electrons are described by plane waves. They tunnel through the left and right barrier's via the quantum well. The potential felt by the electron in various regions is depicted in FIG. 2. A finite voltage bias V is applied across the system. The electron wave in the well experiences multiple reflections due to the presence of barriers (see FIG. 1) and then tunnels out through the right barrier. To calculate the transmission and reflection coefficients we use the transfer matrix method[24]. The transfer matrices of either of the barrier's are calculated by matching the wave functions and their derivatives at the boundaries. To

calculate the transfer matrices we choose the II/III interface as the origin of the coordinate system, and the transfer matrix of the first barrier is given by-

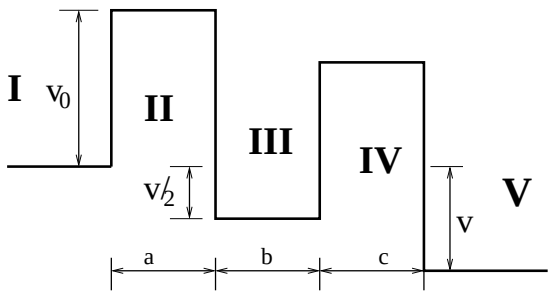


FIG. 2: The double barrier heterostructure.

$$M = \begin{pmatrix} w & z^* \\ z & w^* \end{pmatrix}$$

with $w = \frac{e^{ik_1 a}}{2}((1 + f_{13})cosh(K_2 a) - i(f_{23} - f_{12})sinh(K_2 a))$, and $z = \frac{e^{-ik_1 a}}{2}((1 - f_{13})cosh(K_2 a) - i(f_{23} + f_{12})sinh(K_2 a))$, wherein $f_{13} = k_3/k_1$, $f_{23} = k_3/K_2$, $f_{12} = K_2/k_1$, $K_2 = \sqrt{2m^*(V_0 - E)/\hbar^2}$, and $k_1 = \sqrt{2m^* E/\hbar^2}$. We model incoherent transport only in the well. In the method of Wave Attenuation $k_3 = \sqrt{2m^*(E + V/2)/\hbar^2}$ and we use wave attenuation factor to simulate dephasing as explained below. In the case of Coherent Absorption, the potential in the well is complex and $k_3 = k_p + ik_m = \sqrt{2m^*(E + V/2 - iV_i)/\hbar^2}$. Here V_i is the imaginary part of the potential which is characterized as an incoherent parameter. After obtaining the transfer matrix the S-Matrix[25]of the barrier is calculated by using the formula-

$$S = (\frac{1}{M_{11}}) \begin{pmatrix} M_{21} & detM \\ 1 & -M_{12} \end{pmatrix}$$

wherein M is the transfer matrix of the barrier and indices denote row and column.

The S-Matrix of the second barrier is analogously written. The S-Matrix of the well is -

$$S_w = \begin{pmatrix} e^{ik_3 b}e^{-\alpha b} & 0 \\ 0 & e^{ik_3 b}e^{-\alpha b} \end{pmatrix}$$

in presence of Wave Attenuation, while in presence of coherent absorption[15]the S-Matrix of the well is -

$$S_w = \begin{pmatrix} e^{ik_3 b} & 0 \\ 0 & e^{ik_3 b} \end{pmatrix}$$

with $k_3 = k_p + ik_m = \sqrt{2m^*(E + V/2 - iV_i)/\hbar^2}$, and k_p, k_m are defined as above. In the Wave Attenuation method, an attenuation constant per unit length is introduced in the well, i.e., the factor $e^{-\alpha b}$ in the free propagator amplitudes, every time the electron[7,17] traverses the well of the RTD (see Fig. 1). b is the length of the quantum well. This attenuation factor does not affect the scattering properties of the two neighboring scatterer's as opposed to the Coherent Absorption model. The attenuation constant α represents the incoherence parameter.

Physically the model structure depicted in FIG. 2, shows sharp resonances when the energy of the incident particles is close to that of the quasi-bound state[26]. In practice the barrier's are usually of $Al_xGa_{1-x}As$ and well is of $GaAs$. The important thing realized in such structures is the concept of negative differential resistance(NDR). This is of significance in making oscillator components. But, theoretical models which have tried to model experimental curves have had limited success. Two problems which have hitherto still remained unexplained are - (1). The experimental peak to valley ratios are far below the expected values even in good materials, and (2). time required to store enough carrier's in the well to reach resonant regime seems too long to be compatible with high frequency NDR actually observed[19].

To explain these differences recourse has been made to the effects of inelastic scattering[4,27]. Inelastic scattering is inherent in these structures such as due to phonons, interfaces and other impurities. Modeling inelastic scattering by the models considered above is a convenient way out from the many body treatment needed to explain fully the differences. In case of Wave Attenuation[7] the absorption coefficient α acts as a parameter of incoherent scattering while in case of Coherent Absorption[28] the absorptive potential V_i plays such a role. However, it should be noted that unlike in optics where the number of photons is not conserved so that photons can be truly absorbed and converted into heat. In case of electrons the number of particles has to be conserved, so $\alpha/V_i \neq 0$ does not mean that electrons are absorbed but that they are scattered into different energy channels. Thus the way these are re-injected back into the system so as to preserve current conservation becomes important. The coherent transmission in presence of both Coherent Absorption and Wave Attenuation can be calculated with ease using the S-Matrices depicted above. To calculate the incoherent contribution there are two methods. In the method due to Zohta and Ezawa[28] the total transmission is defined after re-injection as the sum of two contributions, one due

to the coherent part and the other due to the incoherent part, i.e., $T_{tot} = T_{coh} + T_{incoh}$. The incoherent part is calculated as $T_{incoh} = \frac{T_r}{T_l+T_r}A$, herein T_r and T_l are the probabilities for right and left transmission from the region of inelastic scattering and A is the absorbed part which is given by $A = 1 - T_{coh} - R_{coh}$. The quantities T_{coh} and R_{coh} are the coherent transmission and reflection probabilities, respectively. This model has been used by several other authors as well to simulate inelastic scattering[3,4,24]. However, modeling electron transport by this method did not lead to satisfactory answers as the Onsager's symmetry is shown to be violated[29] for the two probe conductance. In the second method due to Brouwer and Beenakker[18], the incoherent transmission is calculated from Büttiker's voltage probe model[13], by mapping the three probe Büttiker's method into a two terminal geometry, and then eliminating the transmission coefficients which explicitly depend on the third probe with the help of unitarity of the S-matrix. They considered a three terminal geometry in which one of the probes is used as a voltage probe. A current $I = I_1 = -I_2$ flows from source to drain. In this model, a fictitious third lead connects the system to a reservoir at chemical potential μ_3 in such a way that no current is drawn ($I_3 = 0$). The $3X3$ unitary S-matrix of the entire system can be written as-

$$S = \begin{pmatrix} r_{11} & t_{12} & t_{13} \\ t_{21} & r_{22} & t_{23} \\ t_{31} & t_{32} & r_{33} \end{pmatrix}$$

Application of the relations[13,17,18]- $I_p = \sum_q G_{pq}[\mu_p - \mu_q], p = 1, 2, 3$ and $G_{pq} = (2e^2/h)T_{pq}$. yields the (dimensionless) two probe conductance $G = \frac{h}{2e^2}\frac{I}{\mu_1-\mu_2}$,

$$G = T_{21} + \frac{T_{23}T_{31}}{T_{31} + T_{32}} \tag{1}$$

The transmission coefficients T_{pq} are related to the elements of the S-Matrix, $T_{pq} = |t_{pq}|^2$.

On elimination of the transmission coefficients which involve the voltage probe using the unitarity of the S - Matrix leads to[18]

$$G = T_{21} + \frac{(1 - R_{11} - T_{21})(1 - R_{22} - T_{21})}{1 - R_{11} - T_{21} + 1 - R_{22} - T_{12}}. \tag{2}$$

Here, G in dimensionless form just denotes the total transmission T_{tot} in accordance with Landauer's formalism, which views Conductance as Transmission[30]. T_{12} and R_{22} are

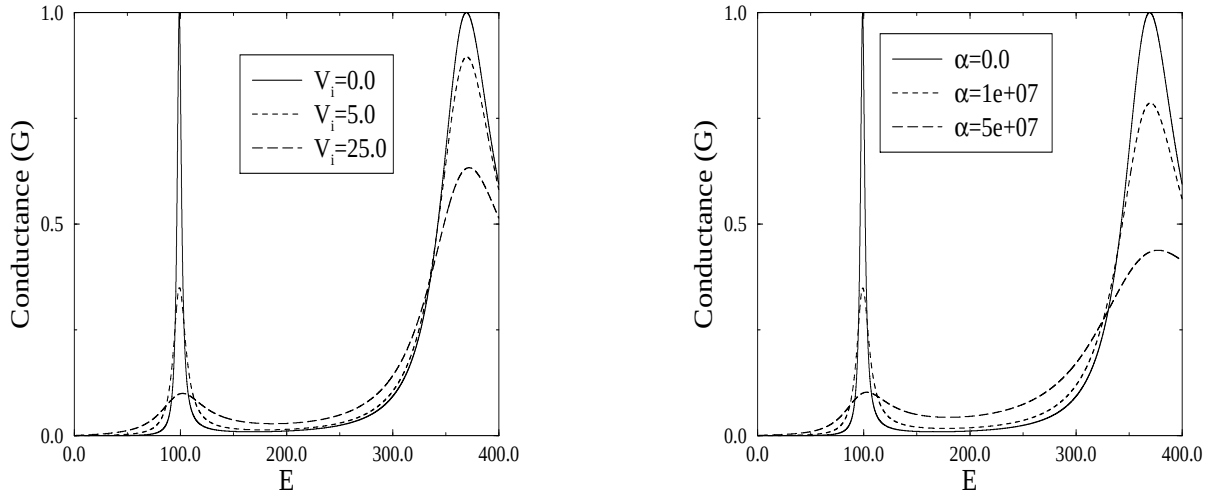


FIG. 3: The total transmission (G) Vs. incident electron energy E (in mev) of a constant imaginary potential(in mev)/attenuation factor(in m^{-1}) in the well, for barrier heights of 0.4 ev and barrier and well widths of 25Åand 50Å.

coherent transmission and reflection when carrier's are incident from the right. Now all the above coefficients are built from the 2X2 S-Matrix.

$$S' = \begin{pmatrix} r_{11} & t_{12} \\ t_{21} & r_{22} \end{pmatrix}$$

The above matrix S' is a sub matrix of the 3X3 unitary S-Matrix of the three port system. Hence matrix S' needn't be unitary, i.e., it can represent the matrix of the non-hermitian or absorbing system. The first term in Eq. 2 represents the conductance contribution from the phase coherent part. The second term accounts for electrons that are re-injected from the phase breaking reservoir, thereby ensuring particle conservation. This part also can be identified as a contribution to the conductance arising from the incoherent processes. Eq. 2 has been obtained by a simple model for reinjecting carrier's which conserves current only in a global way. Another interesting approach may be to reinject carrier's based on the local density of states[31]. For this one has to attach a voltage probe at every point of the system wherein we want to depict incoherent processes. This local approach will be more realistic and will be dealt with in future.

Having defined the total transmission as in Eq. 2, we now focus on the resonant tunneling seen in such devices and the effect of absorption on it. We first look into the effect of

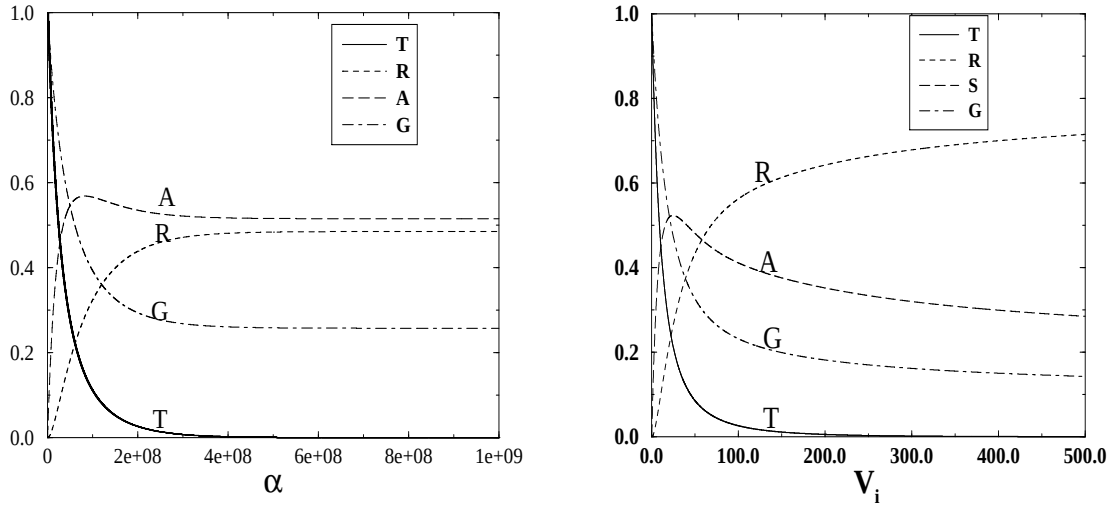


FIG. 4: The Transmission(T), Reflection(R), Absorption(A) and total transmission (G) coefficients at resonant energy (E_r) Vs. strength V_i (in mev) or α (in m^{-1}) in the well, for barrier heights of 0.4 ev and barrier and well widths of 10Åand 50Å. For this system E_r=88.76 mev and applied bias $V = 0.0ev$.

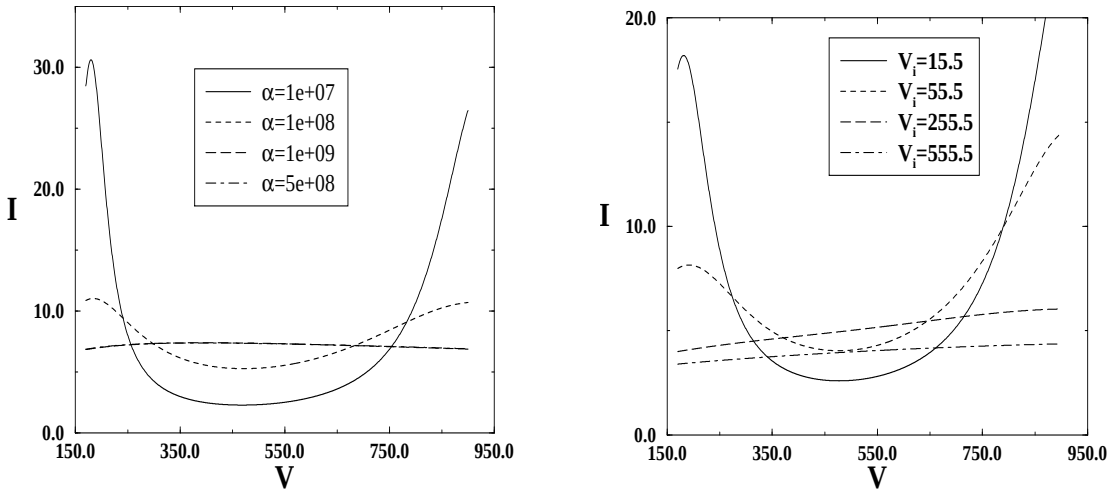


FIG. 5: Tunneling current(I) Vs. applied bias(V in mev) with increase in incoherence imaginary potential (V_i in mev) or attenuation factor (α inm^{-1}). The Fermi energy $E_f = 12.0mev$. The length parameters are same as in FIG. 4.

incoherence on the total transmission (conductance in the linear response regime) in both models of incoherence in the absence of finite bias. We see with increase in incoherence in both models the width of transmission peak increases (see FIG. 3) and height decreases. Also the transmission in the valley region increases in qualitative agreement with prevalent notions of decoherence. In this figure and in all subsequent figures $\alpha = 1e + 05$ implies $1.0X10^5$. We next focus on the total transmission G, coherent transmission T_{21}, coherent reflection R_{11} and absorption defined as $A = 1 - T_{21} - R_{11}$, for both Coherent and Wave Attenuation models of absorption. These are plotted in FIG. 4. We show that in contrast to Coherent Absorption wherein absorption increases and then continuously decreases to zero[20](in the extreme limit of $V_i \to \infty$ the absorber acts as a perfect reflector), in case of Wave Attenuation A increases and then saturates. One of the problems associated with a coherent absorber is that absorption without reflection is not possible and it introduces spurious scattering. A note to be added is that for wider barriers A increases and then decreases (of course saturating) with further increase in incoherence in case of Wave Attenuation also, but this is due to the fact that the prompt part in the reflection amplitude r_1 (see Fig. 1) which is unaffected by dephasing is large, and this interferes with other waves which leads to the non-monotonic behavior seen. This prompt part is also present in case of Coherent Absorption, but unlike Wave Attenuation the A goes to zero in the asymptotic regime($V_i \to \infty$, while in case of Wave Attenuation A always saturates at a value however small. Apart from absorption the true character of these models will be revealed in a comparison of there conductance properties. In case of imaginary potential the total conductance (G) continuously decreases and as $V_i \to \infty$, $G \to 0$ (this limit is not shown in the graph as it goes beyond the scale used), while in-case of Wave Attenuation as $\alpha \to \infty$, G goes to a constant value which depends on the Fermi-energy and other system parameters. Thus we see that the modeling of incoherence by Wave Attenuation is indeed justified as we want the conductance to go to a classical value and not that the conductance itself should vanish, as in the case of Coherent Absorption model. This limiting case clearly indicates that the Wave Attenuation model is more physical than the Coherent Absorption model. In the above analysis it should be noted that, the conductance formula used is valid in the linear response regime.

Another important quantity relevant to the study of electron transport in these double barrier heterostructures is the tunneling current as a function of bias. To determine the

tunneling current we follow the procedure adopted by Tsu and Esaki[19,21], who have obtained in the zero temperature limit the following expressions for tunneling current as a function of the applied bias- (i)for $V \geq E_f$

$$I_t = \frac{em^*}{2\pi^2\hbar^3}\int_0^{E_f} dE(E_f - E)T_{tot} \tag{3}$$

and (ii)for $V < E_f$-

$$I_t = \frac{em^*}{2\pi^2\hbar^3}[V\int_0^{E_f-V} dET_{tot} + \int_{E_f-V}^{E_f} dE(E_f - E)T_{tot}] \tag{4}$$

In FIG. 5, we plot the tunneling current in terms of (I=$I_t/\frac{em^*}{2\pi^2\hbar^3}$)versus applied bias for both Coherent Absorption as well as Wave Attenuation models of absorption. We see that Wave Attenuation models sequential transport in a much better manner than Coherent Absorption. Whereas in case of Coherent Absorption we see that for small increase in V_i sequential contribution (the valley current) increases but for large values of V_i we see that the sequential contribution (or the valley current) actually decreases. This is not so in-case of Wave Attenuation, as sequential transport increases to a defined limit and then saturates as expected.

With this affirmation of the suitability of Wave Attenuation to express sequential transport in RTD's. We now use this model and compare it with some experimental results, and check how far it is accurate. In the paper of Sollner, et.al.[23] wherein the peak to valley ratio 6:1 was obtained, the experiment was performed at 25K with system barrier(AlGaAs) height and length of 230.0 mev and 50$\mathring{A}$, while well(GaAs) width is also 50$\mathring{A}$. We can approximate the relaxation time at 25K to be 10^{-13} secs and Fermi energy for GaAs concentration of $1.0X10^{-18}m^3$ is $18.67mev$. Thus electron mean free path defined to be V_f the Fermi velocity multiplied by the relaxation time is $10^{-8}m$. 2α defined as inverse of mean free path is thus $0.5X10^8m^{-1}$. We find from Eq. 4, the peak to valley ratio to be 3.5:1. Thus our model although, not quite close to experimental results, nevertheless reflects qualitatively the negative differential resistance in Resonant tunneling diodes quite well. This peak-valley ratio is sensitive to the relaxation time and in our analysis we have used the value as quoted in Ref.24.

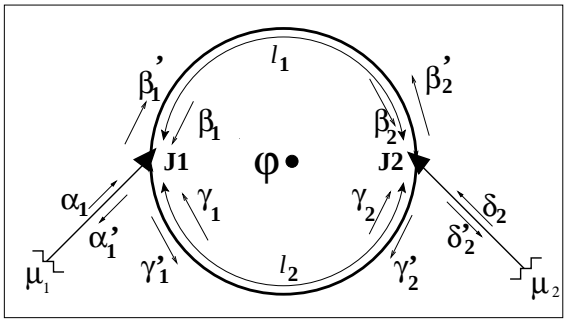


FIG. 6: The asymmetric Aharonov-Bohm ring.

IV. MESOSCOPIC RINGS

In this section we report on the extensively studied non-local phenomena of Aharonov-Bohm oscillations[12,32]. The system under consideration is shown in FIG. 6. It is an asymmetric loop with upper and lower arm lengths l_1 and l_2 and circumference $L = l_1 + l_2$, coupled to two leads which in turn are connected to two reservoirs at chemical potentials μ_1 and μ_2. Inelastic scattering is assumed to be absent in the leads while it is present in the reservoirs, and in the loop we introduce incoherence via Wave Attenuation or Coherent Absorption to simulate inelastic scattering. The S matrix for the left coupler yields the amplitudes $O_1 = (\alpha_1', \beta_1', \gamma_1')$ emanating from the coupler in terms of the incident waves $I_1 = (\alpha_1, \beta_1, \gamma_1)$, and for the right coupler yields the amplitudes $O_2 = (\delta_2', \beta_2', \gamma_2')$ emanating from the coupler in terms of the incident waves $I_2 = (\delta_2, \beta_2, \gamma_2)$. The S-matrix for either of the couplers[33] is given by-

$$S = \begin{pmatrix} -(a+b) & \sqrt{\epsilon} & \sqrt{\epsilon} \\ \sqrt{\epsilon} & a & b \\ \sqrt{\epsilon} & b & a \end{pmatrix}$$

with $a = \frac{1}{2}(\sqrt{(1-2\epsilon)} - 1)$ and $b = \frac{1}{2}(\sqrt{(1-2\epsilon)} + 1)$. Herein, ϵ plays the role of a coupling parameter. The maximum coupling between reservoir and loop is $\epsilon = \frac{1}{2}$, and for $\epsilon = 0$, the coupler completely disconnects the loop from the reservoir. We first consider Wave Attenuation in which inelastic scattering in the arms of the AB interferometer is taken into account by introducing an attenuation constant per unit length in the two arms of the ring, i.e., the factors $e^{-\alpha l_1}$ (or $e^{-\alpha l_2}$) in the free propagator amplitudes, every time the electron[7,17] traverses the upper (or lower) arms of the loop (see Fig. 1), as discussed earlier.

The waves incident into the branches of the loop are related by the S Matrices[34]for upper branch by-

$$\begin{pmatrix} \beta_1 \\ \beta_2 \end{pmatrix} = \begin{pmatrix} 0 & e^{ikl_1}e^{-\alpha l_1}e^{\frac{-i\theta l_1}{L}} \\ e^{ikl_1}e^{-\alpha l_1}e^{\frac{i\theta l_1}{L}} & 0 \end{pmatrix} \begin{pmatrix} \beta_1' \\ \beta_2' \end{pmatrix}$$

and for lower branch-

$$\begin{pmatrix} \gamma_1 \\ \gamma_2 \end{pmatrix} = \begin{pmatrix} 0 & e^{ikl_2}e^{-\alpha l_2}e^{\frac{i\theta l_2}{L}} \\ e^{ikl_2}e^{-\alpha l_2}e^{\frac{-i\theta l_2}{L}} & 0 \end{pmatrix} \begin{pmatrix} \gamma_1' \\ \gamma_2' \end{pmatrix}$$

These S matrices of course are not unitary $S(\alpha)S(\alpha)^\dagger \neq 1$ but they obey the duality[35] relation $S(\alpha)S(-\alpha)^\dagger = 1$. Here kl_1 and kl_2 are the phase increments of the wave function in absence of flux. $\frac{\theta l_1}{L}$ and $\frac{\theta l_2}{L}$ are the phase shifts due to flux in the upper and lower branches. Clearly, $\frac{\theta l_1}{L} + \frac{\theta l_2}{L} = \frac{2\pi\Phi}{\Phi_0}$, where Φ is the flux piercing the loop and Φ_0 is the flux quantum$\frac{hc}{e}$. The transmission and reflection coefficients are given as follows- $T_{21} = |\frac{\delta_2'}{\alpha_1}|^2$, $R_{11} = |\frac{\alpha_1'}{\alpha_1}|^2$, $R_{22} = |\frac{\delta_2'}{\delta_2}|^2$, $T_{12} = |\frac{\alpha_1'}{\delta_2}|^2$ wherein wave amplitudes $\delta_2', \delta_2, \alpha_1', \alpha_1$ are as depicted in FIG. 6.

The coherent transmission coefficient T_{21} from reservoir 1 to 2 is not symmetric under flux reversal and is due to the fact that unitarity has been violated. For calculating the total conductance in case of Coherent Absorption we use Eq. 2, and potential across the ring is imaginary V_1 but we follow the wave guide method[36,37]. The waveguide and S-Matrix methods are not exclusive, in fact the waveguide method is just a special case of the S-Matrix, corresponding to a coupling constant $\epsilon = 4/9$.

In this method (see FIG. 6) the wave functions in the leads are- $\Psi_1 = e^{ikx} + re^{-ikx}$ and $\Psi_2 = te^{ikx}$ for left and right leads respectively. The wavefunctions in the upper and lower arms of the loop are $\Psi_u = a_u e^{ik_1' x} + b_u e^{-ik_2' x}$ and $\Psi_l = a_l e^{ik_2' x} + b_l e^{-ik_1' x}$. Here $k_1' = k' - \frac{\phi}{L}, k_2' = k' + \frac{\phi}{L}$, with $k' = k_p + ik_m$ and $k_p = \frac{k}{\sqrt{2}}\sqrt{1+\zeta}, k_m = \frac{k}{\sqrt{2}}\sqrt{\zeta - 1}$, where $\zeta = \sqrt{1 + (\frac{V_i}{k^2})^2}$.

Thus we have $R_{11} = |r|^2, T_{21} = |t|^2$. For electrons incident from the right lead we adopt a similar procedure to calculate R_{22} and T_{12}. Substituting these coefficients in Eq. 2, we get the total conductance in case of Coherent Absorption. The total conductance (G) in both the cases of absorption obeys Onsager's symmetry while the coherent transmission contribution isn't. The conductance shows flux periodicity of period Φ_0 as expected for ballistic rings[13,32,38]. In the ballistic and asymmetric rings for certain values of the physical parameters $\Phi_0/2$ periodicity has also been seen experimentally and explained using the single channel coherent transport model without dephasing. In our present case as we scan

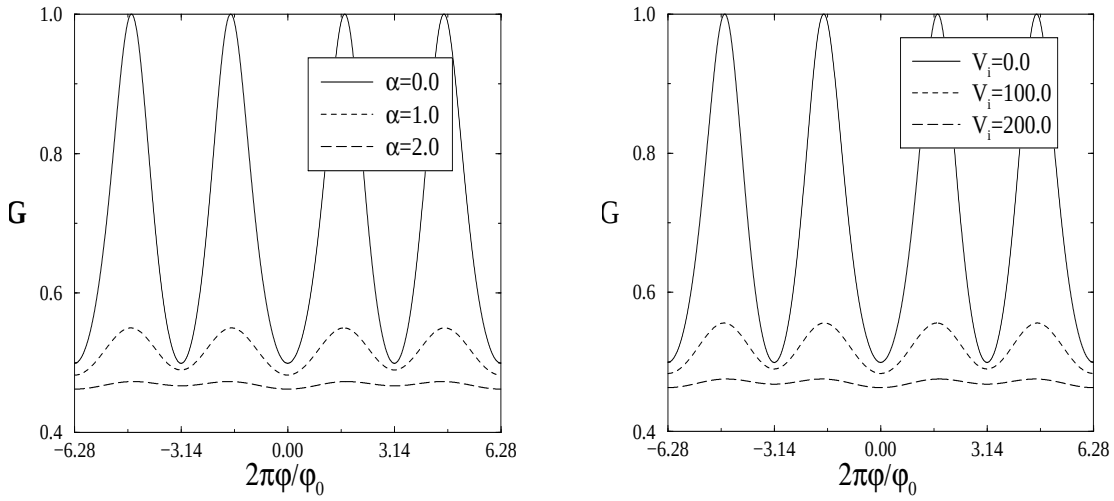


FIG. 7: Comparison of two models of dephasing. Herein the Conductance (absorption in the inset) for the two cases Wave Attenuation(WA) and Coherent Absorption(CA) have been plotted. The parameters (all in dimensionless units) used are $kL = 5.0, l_1/L = 0.375, l_2/L = 0.625, \Phi = 1.0$, and $\epsilon = 4/9$

the range of Fermi wavevector then in some regions we observe $\Phi_0/2$ periodicities a much explored phenomena in these systems as shown in Fig. 7. In both cases, i.e., Coherent Absorption as well as Wave Attenuation, we see that increase in incoherence leads to shifts of exact fermi wavevector wherein $\Phi_0/2$ periodicities occur. Also the visibility defined as the ratio of the difference between maximum and minimum conductances to the sum of maximum and minimum conductances shows similar behavior in either case. In both these cases visibility decreases as a function of incoherence parameter signalling dephasing. Moreover it has been shown that[39] $\Phi_0/2$ periodicity can also be observed in the presence of incoherence which is of-course true for Φ_0 periodicity. To truly bring out the differences between these models of incoherence one has to study the total conductance and absorption as a function of the incoherence parameters.

To this end, in FIG. 8 we plot the total conductance (G) for both the cases. In the case of Coherent Absorption we see that the total conductance (G) continuously decreases and as $V_i \to \infty$, $G \to 0$ (this limit is not shown in the graph as it goes beyond the scale used), while in-case of Wave Attenuation as $\alpha \to \infty$, G goes to a constant value which depends on the Fermi-energy and other system parameters. Thus we see that the modeling of dephasing

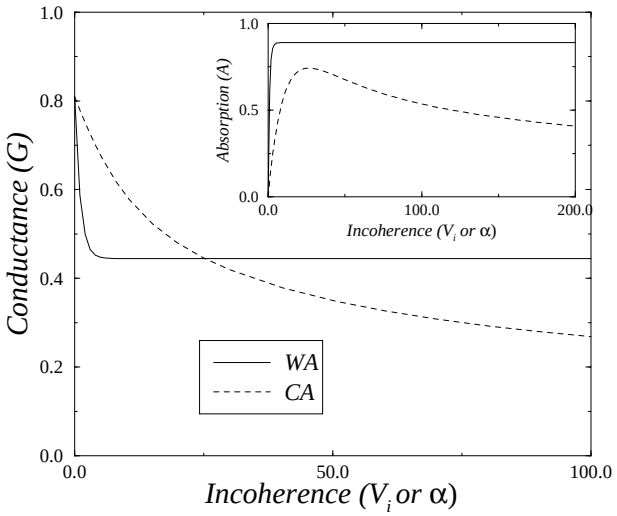


FIG. 8: Comparison of two models of dephasing. Herein the Conductance (absorption in the inset) for the two cases Wave Attenuation(WA) and Coherent Absorption(CA) have been plotted. The parameters (all in dimensionless units) used are $kL = 5.0, l_1/L = 0.375, l_2/L = 0.625, \Phi = 1.0$, and $\epsilon = 4/9$

by Wave Attenuation is indeed justified as we want the AB oscillations to die out and not that the conductance itself should vanish, and this is where Wave Attenuation scores over the Coherent Absorption model. In the figure inset we have depicted the behavior of total absorption in the system A for both the cases for the same physical parameters. As $\alpha \to \infty$ there is a finite absorption in the system as the electron propagates in the medium in this limit whereas absorption in the imaginary potential model is non-monotonic and in the limit $V_i \to \infty$ absorption vanishes. This is due to the fact that in the Coherent Absorption model as $V_i \to \infty$ absorber acts as a perfect reflector as mentioned before. There is no absorption in the medium as the particles do not enter the medium (and hence $G = 0$) obviously which is an unrealistic situation for real systems.

With our model for inelastic scattering we can also study theoretically the effect of incoherence on Fano resonant line shapes. This effect has earlier been seen in various contexts in mesoscopic systems. A recent example being, Fano effect through a quantum dot in an Aharonov-Bohm interferometer by Kobayashi, et.al[40], wherein they see this effect in the nature of the conductance as a function of the gate voltage (Fermi energy). Fano resonances (i.e., asymmetric line shapes) arise when a discrete set of states are coupled to the continuum, these were first proposed by Ugo Fano to explain the characteristic asymmetric line

shapes in nuclear scattering phenomena[41]. Basically it is the effect of interference between two alternatives in which an electron can emerge via resonant localized state or through the continuum. Earlier, in an analysis of a simple quantum dot system taking into account the contribution from direct(non-resonant) path and resonant path the form of the Fano resonance was shown to be[42]

$$G(E) = G_d \frac{|2E + q\Gamma|^2}{4E^2 + \Gamma^2} \tag{5}$$

In the above Eq. 5, $G = |t_d + t_r|^2$ is the conductance with $t_d = e^{i\beta_d}\sqrt{G_d}$ and $t_r(E) = z_r\Gamma/(2E + i\Gamma)$ describing the direct and resonant transmission amplitudes, E the energy, Γ the resonance width, G_d the non-resonant conductance, and $q = i + z_r e^{-i\beta_d}/\sqrt{G_d}$ the complex Fano parameter. It must be remembered that the above form of the Fano line-shape is valid in the absence of dephasing. In the presence of dephasing the form of the total conductance G is as given in Eq. 2. It is claimed earlier[42] that the second part of Eq. 2 will lead to a Breit-Wigner line-shape in the presence of dephasing. We will study this above assertion in our present study of quantum dot in an Aharonov-Bohm ring geometry which is different from that considered earlier[42] using Wave Attenuation method.

In the model we consider, a quantum dot placed on the upper arm of an open Aharonov-Bohm ring. The quantum dot has resonant discrete levels, the interplay of these states with the continuous levels in the Aharonov-Bohm ring gives rise to Fano resonances. We assume the discrete levels of the quantum dot to be having Breit-Wigner forms. Following the formalism of Sun and Lin[43], one can write the pq^{th} element of the 2 X 2 S-Matrix of the quantum dot as-

$$S_{pq} = \delta_{pq} - \frac{i/2}{[\sum_j \frac{\Gamma_j}{E - E_j}]^{-1} + i/2} \tag{6}$$

wherein Γ_j and E_j represent the width and energy of the j^{th} resonant level of the quantum dot while E denotes the Fermi energy and p, q take on values 1 and 2. It should, however, be noted that unlike Sun and Lin, we neglect the intra-dot Coulomb interaction as in Eq. 6 and solve the scattering problem by placing the quantum dot symmetrically in the upper arm of the original Aharonov-Bohm ring(FIG. 6).

In FIG. 9 we plot the Conductance as a function of incident electron energy(in a narrow range) using Eq. 2 for various values of incoherent parameter α. The Conductance shows

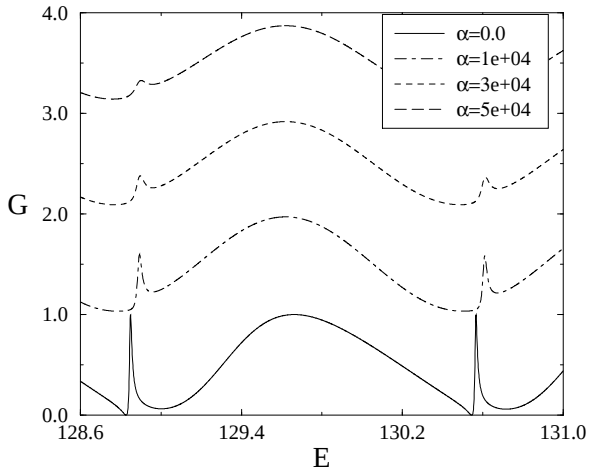


FIG. 9: The Conductance (G) *vs*. E in *mev*. Assuming dot has 5 states with $\Delta E = 20$, $E_j = (2j-1)10$, Γ_j dependent on state j with $\Gamma_1 = 5.0$ and $\Gamma_j = 1.1\Gamma_{j-1}$. The Conductance for increasing values of α in m^{-1} are shifted by 1.0 for clarity. The length parameters of the Aharonov-Bohm ring are $l_1 = l_2 = 10\mathring{A}$ and the dot is symmetrically placed on the upper arm. The coupling strength is 0.5 (maximal) and flux is 0.3 *weber*. The ring as in the experiment is assumed to be of $GaAs$.

Fano line-shapes as one varies the incident electron energy. In this figure the physical parameters are as mentioned in the figure caption. As inelastic scattering parameter α is increased Fano line-shapes broaden and their peak values are reduced. Subtracting the continuum background of the Conductance, we see that the asymmetric Fano line-shapes evolve to symmetric line-shapes corresponding to Lorentzian or Breit-Wigner forms in similarity with experimental observations and also consistent with the treatment of Ref.42. The incoherence parameter 2α is defined as equal to inverse of the mean free path as in the previous section. A representative value of α in FIG. 9, for example $1X10^4$ corresponds to a mean free path of $5X10^{-5}m$ which is in conformity with the millikelvin temperature range at which the experiment has been performed. The complete understanding requires details of physical parameters associated with the real experiment. The complex Fano parameter as defined above also changes with increase in dephasing strength, as seen in Ref.42. Another feature as seen in the experiment is the transition as a function of applied flux, of an asymmetric line-shape to symmetric and then back to asymmetric, further work on these is currently on and will be reported elsewhere.

V. CONCLUSIONS

In this work we have brought out some of the unphysical characteristics associated with the Coherent Absorption model as compared to the Wave Attenuation model which have been used earlier to study dephasing in mesoscopic systems. Both these models are phenomenological in nature and are applied to study transport across Resonant tunneling diodes and Aharonov-Bohm rings. Further we have studied the peak to valley ratios in case of Resonant tunneling diodes, dephasing of magneto-conductance oscillations and Fano resonances. We have shown that the Wave-Attenuation model is consistent with prevalent notions of decoherence.

---

* Electronic address: colin@iopb.res.in

† Electronic address: jayan@iopb.res.in

[1] S. Gasiorowicz, *Quantum Physics* (Wiley Eastern, New York, 2000).

[2] L. I. Schiff, *Quantum Mechanics* (Mc Graw Hill, New York, 1974).

[3] D. Ferry and J. Barker, Appl. Phys. Lett. **74**, 582 (1999).

[4] A. D. Stone and P. A. Lee, Phys. Rev. Lett. **54**, 1196 (1985).

[5] P. Pradhan and N. Kumar, Phys. Rev. B**50**, R9644 (1994).

[6] Sandeep K. Joshi, D. Sahoo and A. M. Jayannavar, Phys. Rev. B**62**, 880 (2000).

[7] Colin Benjamin and A. M. Jayannavar, Phys. Rev. B**65**, 155309 (2002).

[8] S. Anantha Ramakrishna and N. Kumar, preprint cond-mat/0009269.

[9] C. Benjamin and A. M. Jayannavar, Solid State Commun.**121**, 591 (2002).

[10] H. Rauch and J. Summhammer, Phys. Rev. A**46**, 7284 (1992).

[11] R. Landauer, Philos. Mag. **21**, 863 (1970).

[12] Y. Imry, *An introduction to mesoscopic physics* (Oxford, 2001).

[13] M. Büttiker, Phys. Rev. B**33**, 3020 (1986);IBM J. Res. Dev. **32**, 63 (1988).

[14] M. Büttiker in *Resonant Tunneling in Semiconductors, Physics, and Applications*, edited by L. L. Chang, E. E. Mendez and C. Tejedor (Plenum , New York, 1991), p.213.

[15] A. M. Jayannavar, Phys. Rev. B**49**, 14718 (1994); A. K. Gupta and A. M. Jayannavar, Phys. Rev. B**52**, 4156 (1995); S. K.Joshi and A. M. Jayannavar, Int. J. Mod. Phys. B**12**, 1555 (1998);

S. K.Joshi and A. M. Jayannavar, Int. J. Mod. Phys. B**14**, 1669 (2000).

[16] N. A. Mortensen, A. P. Jauho and K. Flensberg, Superlattices and Microstructures **28**, 67 (2000).

[17] S. Datta, *Electron Transport in mesoscopic systems* (Cambridge University press, Cambridge, 1995).

[18] P. W. Brouwer and C. W. J. Beenakker, Phys. Rev. B**55**, 4695 (1997); P. W. Brouwer, Ph.D. thesis, Insttuut-Lorentz, University of Leiden, The Netherlands,1997.

[19] G. Garcia-Calderon, in *The Physics of Low-Dimensional Semiconductor Structures*, edited by Butcher et. al. (Plenum, New York, 1993), p.267.

[20] A. Rubio and N. Kumar, Phys. Rev. B**47**, 2420 (1993).

[21] R. Tsu and L. Esaki, Appl. Phys. Lett. **22**, 562 (1973).

[22] L. L. Chang, L. Esaki and R. Tsu, Appl. Phys. Lett. **24**, 593 (1974).

[23] T. C. L. G. Sollner, W. D. Goodhue, P. E. Tannewald, C. D. Parker and D. D. Peck, Appl. Phys. Lett. **43**, 588 (1983).

[24] Hu Yuming, J. Phys. C **21**, L23 (1988).

[25] D. J. Griffiths, Am. J. Phys. **72**, 3584 (2001).

[26] B. Ricco and M. Ya. Azbel, Phys. Rev. B**29**, 1970 (1984).

[27] M. Johnson and A. Grincwajg , Appl. Phys. Lett. **51**, 1729 (1987).

[28] Y. Zohta and H. Ezawa, J. Appl. Phys. **72**, 3584 (1992).

[29] T. P. Pareek, S. K. Joshi and A. M. Jayannavar, Phys. Rev. B**57**, 8809 (1998).

[30] R. Landauer and Y. Imry, Rev. of Mod. Phys. **71**, S306 (1999).

[31] M. Büttiker, Pramana J. Phys.**58**, 241 (2002).

[32] S. Washburn and R. Webb, Adv. Phys. **35** 375 (1986).

[33] M. Büttiker, Y. Imry and M. Ya. Azbel, Phys. Rev. A**30**, 1982 (1984).

[34] M. Cahay, S. Bandopadhyay and H. Grubin, Phys. Rev. B**39**, R12989 (1986).

[35] J. C. J. Paasschens, T. Sh. Mishirpashaev and C. W. J. Beenakker, Phys. Rev. B**54**, 11887 (1996).

[36] J. B. Xia, Phys. Rev. B**45**, 3593 (1992).

[37] P. S. Deo and A. M. Jayananvar, Phys. Rev. B**50**, 11629 (1994); A. M. Jayananvar and P. S. Deo, Phys. Rev. B**49**, 13685 (1994); T. P. Pareek, P. S. Deo and A. M. Jayananvar, Phys. Rev. B**52**, 14657 (1995); Sandeep K. Joshi, D. Sahoo and A. M. Jayannavar, Phys. Rev. B**64**,

075320 (2001).

[38] Y. Gefen, Y. Imry, M. Ya. Azbel, Phys. Rev. Lett. **52**, 129 (1984).

[39] C. Benjamin, S. Bandyopadhyay and A. M. Jayannavar, preprint cond-mat/0205662, Solid State Commun.(2002) in press.

[40] K. Kobayashi, H. Aikawa, S. Katsumoto and Y. Iye, Phys. Rev. Lett. **88**, 256806 (2002).

[41] U. Fano, Phys. Rev. **124**, 1866 (1961).

[42] A. A. Clerk, X. Waintal and P. W. Brouwer, Phys. Rev. Lett. **86**, 4636 (2001).

[43] Q. Sun and T. Lin, Eur. Phys. J B **5**, 913 (1998).